Exploring Ozone Production Sensitivity to NO<sub>x</sub> and VOCs in the New York City Airshed in the Spring and Summers of 2017-2019 Abby E. Sebol<sup>1</sup>, Timothy P. Canty<sup>1</sup>, Glenn M. Wolfe<sup>2</sup>, Reem Hannun<sup>2,3</sup>, Allison M. Ring<sup>1</sup>, Xinrong Ren<sup>1,4</sup> <sup>1</sup>Department of Atmospheric and Oceanic Science, University of Maryland, College Park <sup>2</sup>Atmospheric Chemistry and Dynamics Laboratory, NASA Goddard Space Flight Center <sup>3</sup>Department of Geology and Environmental Science, University of Pittsburgh <sup>4</sup>Air Resources Laboratory, National Oceanic and Atmospheric Administration Corresponding author: Abby E. Sebol asebol@umd.edu 4254 Stadium Dr, College Park, MD 20742

# **Highlights:**

- Ozone production is faster in the morning than in the afternoon.
- VOC-limited ozone production is frequent along the Connecticut coastline and in NYC.
- Ozone production sensitivity to biogenic and anthropogenic VOC varies with season and time of day.
- Greater ozone production is calculated using MCMv3.3.1 compared to CB6r2, though both mechanisms exhibit similar NO<sub>x</sub> sensitivity.

## **Abstract:**

Reducing ozone in the New York City (NYC) region requires understanding the nonlinearity of ozone production (PO<sub>3</sub>) and its sensitivity to volatile organic compounds (VOCs) and nitrogen oxides ( $NO_x = NO_2 + NO$ ). Using observations from the Long Island Sound Tropospheric Ozone Study (LISTOS) in the late spring and summers of 2017-2019 and a 0-D box model, we test the sensitivity of PO<sub>3</sub> to ozone precursors. PO<sub>3</sub> is greater in the morning than the afternoon due to increased concentrations of NO<sub>2</sub> and VOC. This diurnal variation in PO<sub>3</sub> is enhanced in the late summer. Based on the model response of PO<sub>3</sub> to changes in initial NO<sub>2</sub>, 14% of samples are within a VOC-limited regime. The metric LRO<sub>x</sub>/LNO<sub>x</sub>, which compares the radical loss rates via selfreaction to their reaction with NO<sub>2</sub>, indicates an additional 17% of samples are in transition between NO<sub>x</sub> and VOC-limited regimes (0.30 < LRO<sub>x</sub>/LNO<sub>x</sub> < 1). We often find PO<sub>3</sub> to be VOClimited in NYC and along the Connecticut coastline (I-95 corridor). In these samples, PO<sub>3</sub> is most sensitive to isoprene, propene, and isopentane, and individual VOCs have strong diurnal and seasonal variations. We further compare PO<sub>3</sub> calculations using the near explicit Master Chemical Mechanism (MCMv3.3.1) and Carbon Bond 6 revision 2 (CB6r2) for a more direct link to regulatory air quality models. Modeled PO<sub>3</sub> is 20% greater in MCMv3.3.1, due largely to the speciation of VOC and organic peroxy radicals, however the bounds of LRO<sub>x</sub>/LNO<sub>x</sub> used to determine the transition range between PO<sub>3</sub> regimes remain the same.

# **Keywords:**

- Air Quality; Long Island Sound Tropospheric Ozone Study (LISTOS); Framework for 0-D
- Atmospheric Modeling (F0AM); Ozone production; NO<sub>x</sub>; VOCs

## **Abbreviations**

- 59 LISTOS, Long Island Sound Tropospheric Ozone Study; PO<sub>3</sub>, ozone production; VOC, Volatile
- 60 Organic Compound; F0AM, Framework for 0-D Atmospheric Modeling; MCM, Master Chemical
- Mechanism version 3.3.1; CB6r2, Carbon Bond mechanism version 6 revision 2.

# 1. Introduction

Surface ozone is responsible for one million premature deaths globally every year (Anenberg et al., 2010; Malley et al., 2017). Despite significant reductions in ozone precursors in recent decades, an estimated 120 million people live in areas that surpass the EPA's national air quality standard for ozone of 70 ppb over an 8-hour average. There are 20 million people in the New York (NY)-New Jersey (NJ) -Connecticut (CT) region which is classified by the EPA as 'moderately' out of attainment (EPA, 2023).

Ozone production (PO<sub>3</sub>) in the troposphere is driven by the oxidation of carbon monoxide (CO) and volatile organic compounds (VOCs) in the presence of nitrogen oxides (NO<sub>2</sub> + NO = NO<sub>x</sub>). PO<sub>3</sub> is nonlinear with respect to precursor concentrations due to the relative importance of radical termination reactions. In relatively low NO<sub>x</sub> environments (NO<sub>x</sub>-limited regime), radical self-reaction is the predominant termination step:

76 
$$HO_2 + HO_2 \rightarrow H_2O_2 + O_2$$
 (R1)

$$HO_2 + RO_2 \rightarrow ROOH + O_2$$
 (R2)

$$RO_2 + RO_2 \rightarrow ROOR + O_2$$
 (R3)

Under these conditions, lowering NO<sub>x</sub> concentrations will decrease PO<sub>3</sub>. In relatively high NO<sub>x</sub>
environments (VOC-limited regime), the formation of nitric acid is the main terminating
reaction:

$$NO_2 + OH + M \rightarrow HNO_3 + M$$
 (R4)

Under this regime, lowering NO<sub>x</sub> concentrations will increase PO<sub>3</sub>. The transition between regimes occurs when NO<sub>x</sub> decreases to the point where the rates of R1-R3 become greater than R4.

Several metrics are available to classify the PO<sub>3</sub> regime. The Empirical Kinetic Modeling Approach (EKMA) utilizes a 0-dimensional box model constrained by observations or estimated emissions of NO<sub>x</sub> and VOCs. Varying input concentrations or emissions in the model tests the sensitivity of PO<sub>3</sub> to effectively map the NO<sub>x</sub> and VOC space.

Another method involves comparing radical loss rates of self-reaction (LRO<sub>x</sub>, sum of reactions R1-R3) to the reaction with NO<sub>2</sub> (LNO<sub>x</sub>, reaction R4). If ozone production was only determined by radical destruction, the transition point would be where  $LRO_x/LNO_x = 1$ . However, past studies have highlighted a discrepancy between these techniques. The value of  $NO_x$  where  $LRO_x/LNO_x = 1$  is less than the value of  $NO_x$  at the peak  $PO_3$  transition point determined by the EKMA isopleths. At the transition point on the EKMA curves, LRO<sub>x</sub>/LNO<sub>x</sub> is estimated to be 0.37 by Kleinman et al., 2001. Schroeder et al., 2017 estimates this threshold to be 0.25-0.45 with a median of 0.35, based on observations from several U.S. urban areas.

Effective NO<sub>x</sub> controls have transitioned much of the NYC region to a NO<sub>x</sub>-limited regime (He et al., 2020; Roberts et al., 2022). Complex and changing emission sources, however, challenge efforts to quantify spatial and temporal variations of PO<sub>3</sub> in this region (Chen et al., 2019). Anthropogenic emissions of NO<sub>x</sub> and VOCs are transported into the region via prevailing westerly winds (long range transport) or emitted directly from NYC (local emissions) and transported downwind. Local sources include industrial and manufacturing activity, energy production, traffic and volatile chemical products (personal care products, pesticides, paints, etc.) (McDonald et al., 2018; Gkatzelis et al., 2021; Coggon et al., 2021; Oliveira et al., 2023).

Biogenic VOCs (BVOC) also contribute to total atmospheric loadings in NYC from forested regions (Chen et al., 2019). Season and time of day affect the relative impact of BVOC (Ring et al., 2023).

We use airborne observations of reactive gases acquired in and around NYC in the spring and summers of 2017-2019 to derive spatial and temporal patterns in ozone production. We constrain a box model with these observations to test the sensitivity of PO<sub>3</sub> to changes in initial concentrations of NO<sub>x</sub> and individual VOCs. We compare this sensitivity between morning and afternoon samples as well as seasonal differences. With these results, we investigate the transition point between NO<sub>x</sub> and VOC-limited air samples using the slope of the PO<sub>3</sub> curve and LRO<sub>x</sub>/LNO<sub>x</sub>. We estimate PO<sub>3</sub> using both nearly explicit and lumped mechanisms to investigate the differences in their respective RO<sub>2</sub> and PO<sub>3</sub> representation. This comparison puts our results into context with regulatory air quality modeling which utilizes lumped mechanisms.

### 2. Methods

# 2.1 Aircraft Observations

This study analyzes aircraft data from two flight campaigns. The Long Island Sound Tropospheric Ozone Study (LISTOS: <a href="https://www-air.larc.nasa.gov/missions/listos/">https://www-air.larc.nasa.gov/missions/listos/</a>) was a multi-agency project to investigate air quality within the NY metropolitan area during July and August 2018 and 2019. The Regional Atmospheric Measurement Modeling and Prediction Program (RAMMPP; http://www.atmos.umd.edu/~rammpp), led by the University of Maryland, is a long-term effort to study air quality in the Eastern United States through both in situ

 observations and large-scale chemical modeling. We use RAMMPP data collected in May 2017 within the same study domain as LISTOS (Fig. 1).

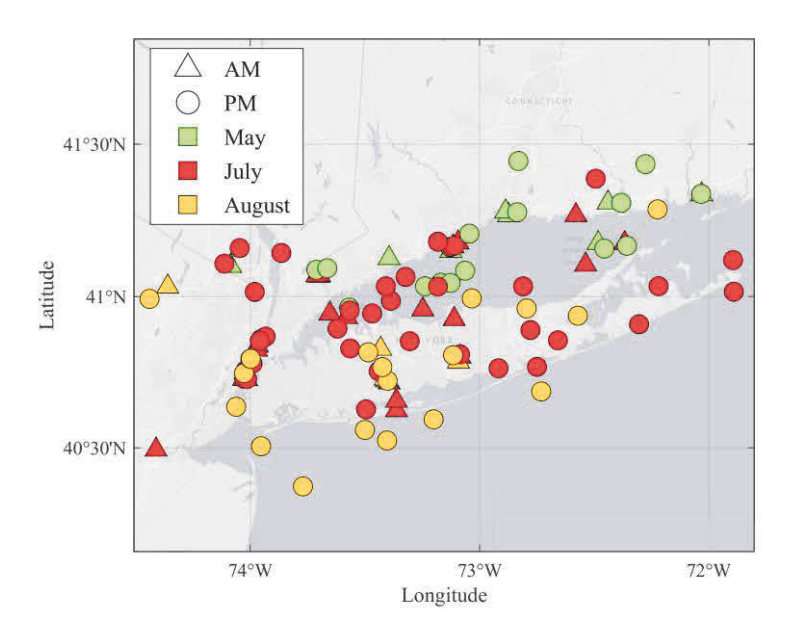


**Figure 1:** Location of the LISTOS whole air samples. Triangle markers indicate morning observations (before local noon), circles for the afternoon observations (after local noon). Green, red, and yellow are observations taken in May, July, and August, respectively. All observations are taken below 1.5 km.

Flights utilized a CESSNA 402B aircraft equipped with in situ measurements of ozone, NO, NO<sub>2</sub>, CO, SO<sub>2</sub>, CH<sub>4</sub>, CO<sub>2</sub>, and meteorological parameters, including ambient temperature, relative humidity, pressure, wind speed and direction. A complete description of the aircraft instrumentation can be found in Ren et al. (2018). Some flights in 2018 and 2019 also included observations of formaldehyde (HCHO) from the NASA Compact Airborne Formaldehyde Experiment (CAFE) (St Clair et al., 2019).

The whole air samples collected in canisters were analyzed for VOC concentrations offline with Gas Chromatography- Flame Ionization Detection or Mass Spectrometry. Table S1 lists all reported VOCs. All continuously monitored state variables and chemical species were averaged over the whole air sampling window, typically spanning about two minutes.

A total of 118 samples were taken from 2017 to 2019 over the Long Island Sound (LIS) region; here we only consider the 107 samples that were accompanied by valid NO<sub>2</sub> observations and within the domain of interest (Fig. 1). Of these, 34 were collected in the morning (before 12:00 EDT) and 73 in the afternoon (after 12:00 EDT). All were collected at altitudes of 1.5 km or less. Simultaneous HCHO observations are available for 41 of 107 samples.

# 2.2 Box Model

We use the Framework for 0-D Atmospheric Modeling (F0AM) version 3 (Wolfe et al., 2016) to model PO<sub>3</sub>. Simulations are constrained to observations of temperature, pressure, relative humidity, CH<sub>4</sub>, NO<sub>2</sub>, NO, O<sub>3</sub>, SO<sub>2</sub>, and all measured VOCs except HCHO. Unobserved species are initialized at 0 ppb. HCHO observations are used for sensitivity tests as described in Supplemental Text S1 and are not included in the box model as they are not available for all samples.

Photolysis frequencies are estimated using F0AM's "hybrid" parameterization, which combines solar spectra from the Tropospheric Ultraviolet and Visible Radiation Model (TUV) with quantum yields and cross sections from the IUPAC (Atkinson et al., 2004; Atkinson et al., 2006) and JPL (Sander et al., 2011) databases. Given inputs of solar zenith angle (SZA), altitude, overhead ozone, and surface albedo, look up tables provide previously calculated photolysis frequencies (j values). We assume clear sky conditions and constant overhead ozone (325 DU) and surface albedo (0.2).

We utilize both the Master Chemical Mechanism version 3.3.1 (hereafter referred to as MCM; Jenkin et al., 2015) and Carbon Bond 6 version 2 (CB6r2; Hildebrandt Ruiz and

Yarwood, 2013) chemical mechanisms. We implement a subset of the full MCM including 13,424 reactions and 4,475 species, tailored to available observations. CB6r2 contains 216 reactions and 77 explicit species or families of species. Rate constants for reactions involving the families in CB6r2 are often based on the rate of a single, representative species (Gery et al., 1989). We include CB6r2 for contrast with the explicit MCM and to more directly link the results to regulatory air quality models. Unless otherwise stated, results represent output from MCMbased simulations. Some measured VOCs are not included in either chemical mechanism (Table S1).

For each set of observations, we run F0AM for 24 hours at 15-minute time steps with photolysis frequencies evolving along the diurnal cycle. We initialize and hold all observed species constant. Total NO<sub>x</sub> is held constant while NO and NO<sub>2</sub> are allowed to partition internally. A physical loss lifetime of 24 hours is applied to all species to prevent build-up of long-lived species. One day of model simulations may not be sufficient to reach full steady state in all cases, but model results and our conclusions do not change significantly for longer integration times. To test this, we extended the integration time to the point when OH, HO<sub>2</sub>, and HCHO reached convergence, defined as a day-to-day change of less than 0.1%. On average, this took four days of integration time and reduced PO<sub>3</sub> by 6%.

This simulation framework is consistent with prior box model studies of PO<sub>3</sub> and VOC chemistry (Crawford et al., 1999; Olson et al., 2001; Olson et al., 2004; Schroeder et al., 2016; Mazzuca et al., 2016; Marvin et al., 2017; Schroeder et al., 2017; Souri et al., 2020; Lindsay et al., 2022). Instantaneous PO<sub>3</sub> is calculated at the end point of each model run.

$$PO_3 = k_{NO,HO2}[NO][HO_2] + \sum (k_i[NO][RO_2]_i)$$
 -

 $(k_{OH,O3}[OH][O_3] + k_{HO2,O3}[O_3][HO_2] + k_{NO2,OH}[NO_2][OH] + \sum (k_i[O_3][VOC]_i) + j[O_3])$ (5)

where the first two terms are production terms and the last 5 are loss terms. We calculate

LRO<sub>x</sub>/LNO<sub>x</sub> using reactions R1- R4. OH reactivity (OHr) is defined as

$$OHr = \sum k_{i,OH}[VOC]_i$$
 (6)

where k<sub>i,OH</sub> is the rate constant for the reaction between hydroxyl (OH) and each individual VOC and [VOC]<sub>i</sub> is the corresponding concentration.

Several sensitivity tests probe the response of PO<sub>3</sub> to NO<sub>x</sub> and VOCs. To generate traditional PO<sub>3</sub> curves as a function of NO<sub>x</sub>, we modify initial NO<sub>2</sub> from 0.01 to 30 ppb while holding VOCs constant. Separately, we test local VOC sensitivity by changing the initial concentrations of VOCs by  $\pm 1\%$  while holding NO<sub>x</sub> constant.

#### 3. Results and Discussion

3.1 PO<sub>3</sub> Sensitivity to NO<sub>x</sub>

### 3.1.1 Transition Region

Fig. 2 shows 107 PO<sub>3</sub> curves individually generated from each sample by varying initial NO<sub>2</sub>. Median PO<sub>3</sub> is represented as the bold blue line. On average, peak PO<sub>3</sub> is 23 ppb/hr and occurs at a NO<sub>2</sub> mixing ratio of 5.1 ppb. Median observed NO<sub>2</sub> (black circle) is 1.8 ppb and corresponds to median PO<sub>3</sub> of 13 ppb/hr. This value of PO<sub>3</sub> corresponding to observed NO<sub>2</sub> is hereafter referred to as 'control PO3'.

Based on d[PO<sub>3</sub>]/d[NO<sub>2</sub>] (henceforth referred to as the 'slope') at each observed NO<sub>2</sub> point, 92 samples (86%) are within NO<sub>x</sub>-limited regime and 15 samples (14%) are within VOC-

 limited regime, where NO<sub>x</sub>-limited is defined as a positive slope and VOC-limited is defined as a negative slope. There is a difference in the control PO<sub>3</sub> between regimes; NO<sub>x</sub>-limited regimes have a median of 14.5 ppb/hr at the observed NO<sub>2</sub> and VOC-limited regimes have a median of 20.5 ppb/hr.

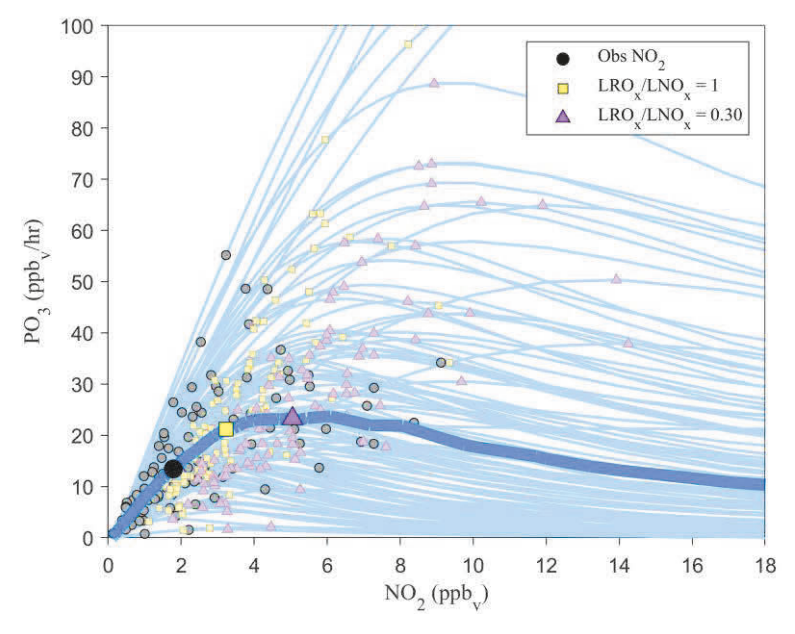


**Figure 2:** Individual PO<sub>3</sub> (ppb/hr) as a function of initial NO<sub>2</sub> concentration (n=107). The bold blue line represents the median PO<sub>3</sub> curve. Each line includes the observed NO<sub>2</sub> (black/gray circle),  $LRO_x/LNO_x = 1$  (yellow square), and  $LRO_x/LNO_x = 0.30$  (pink triangle).

We use LRO<sub>x</sub>/LNO<sub>x</sub> to investigate the magnitude of the PO<sub>3</sub> response to changes in both VOCs and NO<sub>x</sub>. At the peak of the PO<sub>3</sub> curves, LRO<sub>x</sub>/LNO<sub>x</sub> ranges from 0.15 to 0.54 (Fig. S1) and has an average value of 0.30 (pink triangle). Schroeder et al., 2017 provides a range of 0.25-0.45 for LRO<sub>x</sub>/LNO<sub>x</sub> at peak PO<sub>3</sub> using data over several years and multiple urban cities in the United States. Different VOC observations are likely responsible for the variation in average peak value. Despite the diverse environments, the value of LRO<sub>x</sub>/LNO<sub>x</sub> at the peak PO<sub>3</sub>, does not drastically change.

LRO<sub>x</sub>/LNO<sub>x</sub> is equal to one (vellow square) at NO<sub>x</sub> values below the peak of the PO<sub>3</sub> curve. This is the point at which the radical removal rates via peroxide and nitric acid formation are equal. The relationship between slope and LRO<sub>x</sub>/LNO<sub>x</sub> is illustrated further in Fig. S2. We define the range  $0.3 \le LRO_x/LNO_x \le 1$  as the "transition region" between  $NO_x$  and VOClimited regimes. In this transition region, reductions in NO<sub>x</sub> and VOC both reduce PO<sub>3</sub>, but VOCs have a greater impact per molecule. In a sense, PO<sub>3</sub> is neither NO<sub>x</sub> nor VOC-limited in this range. Using this definition, 17 observations (16%) are in transition. This method of defining transition emphasizes the importance of VOCs along with NO<sub>x</sub> in lowering ozone production and provides greater detail in defining the shift between NO<sub>x</sub> and VOC-limited regimes.

3.1.2 Spatial variability of PO<sub>3</sub> regime

Fig. 3 maps the designated PO<sub>3</sub> regime as defined by LRO<sub>x</sub>/LNO<sub>x</sub> (Fig. S3 shows a map of the PO<sub>3</sub> regime as defined by the sign of the slope). As previously stated, most of the samples (73% based on LRO<sub>x</sub>/LNO<sub>x</sub>) are in a NOx-limited regime (red circle). This is especially true over Long Island and the Long Island Sound. However, along the Hudson River and CT coastline (I-95 corridor), we find several samples with a VOC-limited regime (blue triangle) or in transition (white square). Transportation and other industrial activities emit sufficient NO<sub>x</sub> to sustain a VOC-limited regime. Coastal meteorology may also play a role due to the recirculation of marine air through sea breezes (Loughner et al., 2014; Mazzuca et al., 2017; Mazzuca et al., 2019; Couillard et al., 2021).

3.1.3 Diurnal and Seasonal Variability

Past studies show that PO<sub>3</sub> is faster and more VOC-limited in the morning than afternoon due to a lower boundary layer in the morning which concentrates ozone precursors closer to the surface (Chen et al., 2010; Mao et al., 2010; Baier et al., 2015; Mazzuca et al., 2016; Strode et al., 2019; Ring et al., 2023). PO<sub>3</sub> also increases in the later summer due to greater emissions of reactive BVOC (Coates et al., 2016).

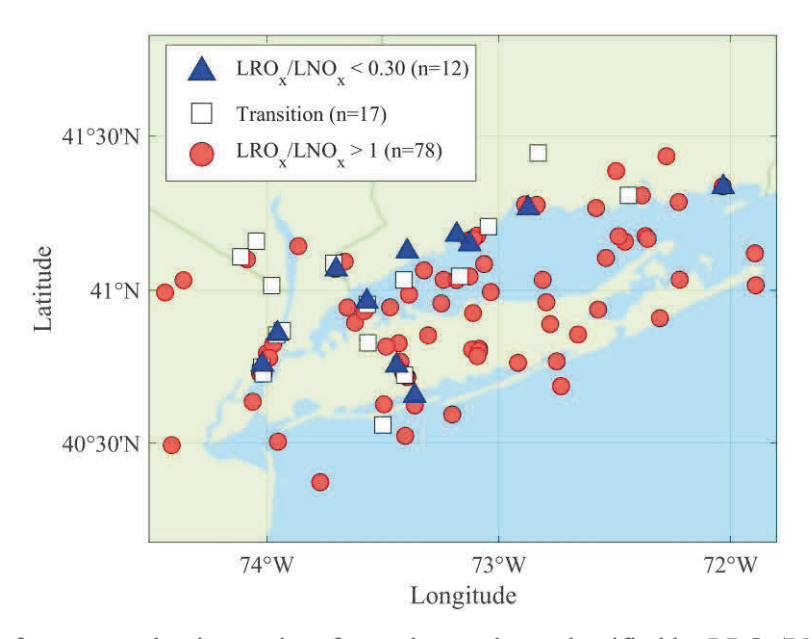


**Figure 3:** Map of ozone production regime for each sample as classified by  $LRO_x/LNO_x$  at observed  $NO_2$ . Blue triangles represent a VOC-limited regime and red circles a  $NO_x$  limited regime. The  $LRO_x/LNO_x$  transition region between 0.30 and 1 is represented by white squares.

In Fig. 4, PO<sub>3</sub> is grouped by month and time of day (See Fig. S4 for only the AM and PM groupings). Here, the mean PO<sub>3</sub> curves for the entire month (blue) as well as AM (purple) and PM (orange) are included. The mean observed NO<sub>2</sub> values at their corresponding control PO<sub>3</sub> are marked as black circles.

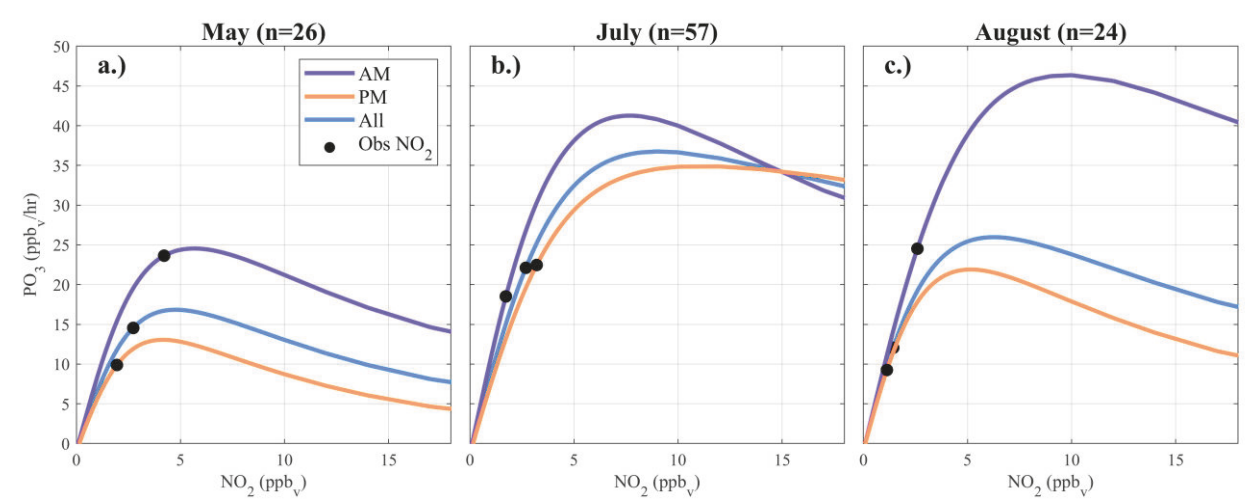


**Figure 4:** Mean PO<sub>3</sub> in (a) May (n = 26), (b) July (n = 57), and (c) August (n = 24). Each month includes AM (purple), PM (orange) and all samples (blue). Observed NO<sub>2</sub> are indicated by black circles.

Peak PO<sub>3</sub> is greater in the morning than the afternoon for all months with August having the most apparent diurnal difference. Control PO<sub>3</sub> is greater in the morning in the months of May and August while July has slightly higher control PO<sub>3</sub> in the afternoon due to greater observed NO<sub>2</sub> concentrations in this month. Photolysis frequency variability plays a minor role in these differences as flights typically occurred during daytime fair-weather conditions. Calculated jNO<sub>2</sub> and jO<sup>1</sup>D correlate poorly with PO<sub>3</sub> (R<sup>2</sup> is 0.20 and 0.19, respectively).

The proportion of VOC-limited PO<sub>3</sub> samples is similar for both morning and afternoon. In the morning 5 of the samples are in a VOC-limited regime (14%) and in the afternoon 10 are in a VOC-limited regime (13%). Greater VOC concentrations in the morning shift the peak PO<sub>3</sub> upwards and towards higher NO<sub>2</sub> values. While morning NO<sub>2</sub> is on average greater than the afternoon, peak PO<sub>3</sub> is not exceeded more frequently.

May has the lowest potential for ozone production and is most likely to be in transition or in a VOC-limited regime. May exhibits the lowest peak PO<sub>3</sub> (17ppb/hr) and based on the average observed NO<sub>2</sub>, most samples are near the maximum potential of PO<sub>3</sub>. There is greater peak PO<sub>3</sub> in the summer months; July and August have an average peak PO<sub>3</sub> of 37 ppb/hr and 26 ppb/hr,

respectively. Increased isoprene emissions in the summer boosts total OH reactivity and (given sufficient NO<sub>2</sub>) increases potential PO<sub>3</sub>. However, these months are not experiencing their maximum potential of PO<sub>3</sub> due to lower observed NO<sub>2</sub>. The average control PO<sub>3</sub> is greatest in July (22 ppb/hr) while May and August have similar values (15 and 12 ppb/hr, respectively).

Photolysis frequencies are similar across all months implying that solar radiation does not impact the seasonal pattern of modeled PO<sub>3</sub> in this study. The median values of jNO<sub>2</sub> for May, July, and August are 0.009, 0.011, and 0.011 s<sup>-1</sup>, respectively. Median values of jO<sup>1</sup>D are 1.9x10<sup>-5</sup>, 2.8 x10<sup>-5</sup>, and 2.3 x10<sup>-5</sup> s<sup>-1</sup> in the same order. Note that this is only an approximation of typical clear sky conditions for these periods. Median temperatures of the aircraft observations are similar in all months, 26.6°C, 28.2°C, and 25.8°C suggesting that temperature-dependent reaction rate coefficients are also not likely to be driving the seasonal variation in PO<sub>3</sub>.

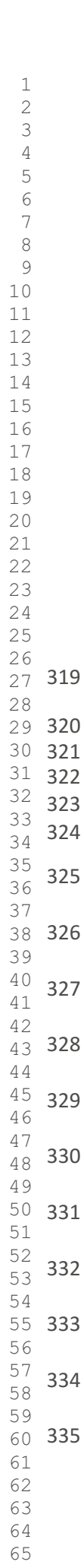
May has the largest percentage of PO<sub>3</sub> that is VOC-limited (27% based on slope) and in transition (19% using LRO<sub>x</sub>/LNO<sub>x</sub>). For these cases, lowering VOC concentrations would lead to a greater reduction, per molecule, of PO<sub>3</sub>. On average, morning PO<sub>3</sub> in May is VOC-limited while the afternoon is NO<sub>x</sub>-limited but near the transition. PO<sub>3</sub> in July is mostly NO<sub>x</sub>-limited (14%), and in August is completely NO<sub>x</sub>-limited. These months have the highest isoprene emissions and total OH reactivity. These results highlight that ozone control strategies must consider seasonally varying chemistry.

May observations were predominantly taken in the Long Island Sound and near the CT coast, while July and August samples were more concentrated over Long Island and NYC (Fig.1). Comparison of spatial subsets for each month suggests that averages are representative of the domain even though sampling does not perfectly overlap (Text S1).

# 3.2 VOC Sensitivity

Fig. 5 shows PO<sub>3</sub> sensitivity for VOCs to which modeled PO<sub>3</sub> is most sensitive, focusing on the 15 samples with VOC-limited PO<sub>3</sub>. Initial VOC concentrations were altered ±1%, one species at a time and the corresponding percent change in PO<sub>3</sub> from the base simulations observations is calculated. Species with less than 3 valid observations in this subset are not included. Fig. 5a shows the diurnal variation of VOC sensitivity and Fig. 5b shows the seasonal variation between May and July (there were no samples within a VOC-limited regime in August). By defining PO<sub>3</sub> sensitivity to a percent change in initial concentrations, this metric inherently accounts for both the quantity and reactivity or each VOC. The percent change of PO<sub>3</sub> due to percent change of NO<sub>2</sub>, based on the NO<sub>2</sub> sensitivity results (Fig. 2), is included for comparison. Because we focus on a subset with VOC-limited PO<sub>3</sub>, the sensitivity of PO<sub>3</sub> to NO<sub>2</sub> is negative by definition.

As shown in Fig. 5, PO<sub>3</sub> is most sensitive to isoprene. A 1% change of isoprene causes, on average, a 0.28% change in PO<sub>3</sub>. Isoprene comprises 7% of the total OH reactivity, the largest constituent of the measured organics, and 0.73% of total observed non-methane VOC on a permolecule basis. The next most important VOC for PO<sub>3</sub> is propene which causes a 0.12% change in PO<sub>3</sub> per percent change in initial concentration. Propene makes up 1.9% of total OH reactivity and 0.72% of total non-methane VOC mixing ratio. While sharing a similar percentage of total concentration as propene, isoprene is a much more reactive VOC and will produce more ozone per molecule. After isoprene and propene, PO<sub>3</sub> is most sensitive to isopentane, toluene, and butane, all of which are anthropogenic VOC.



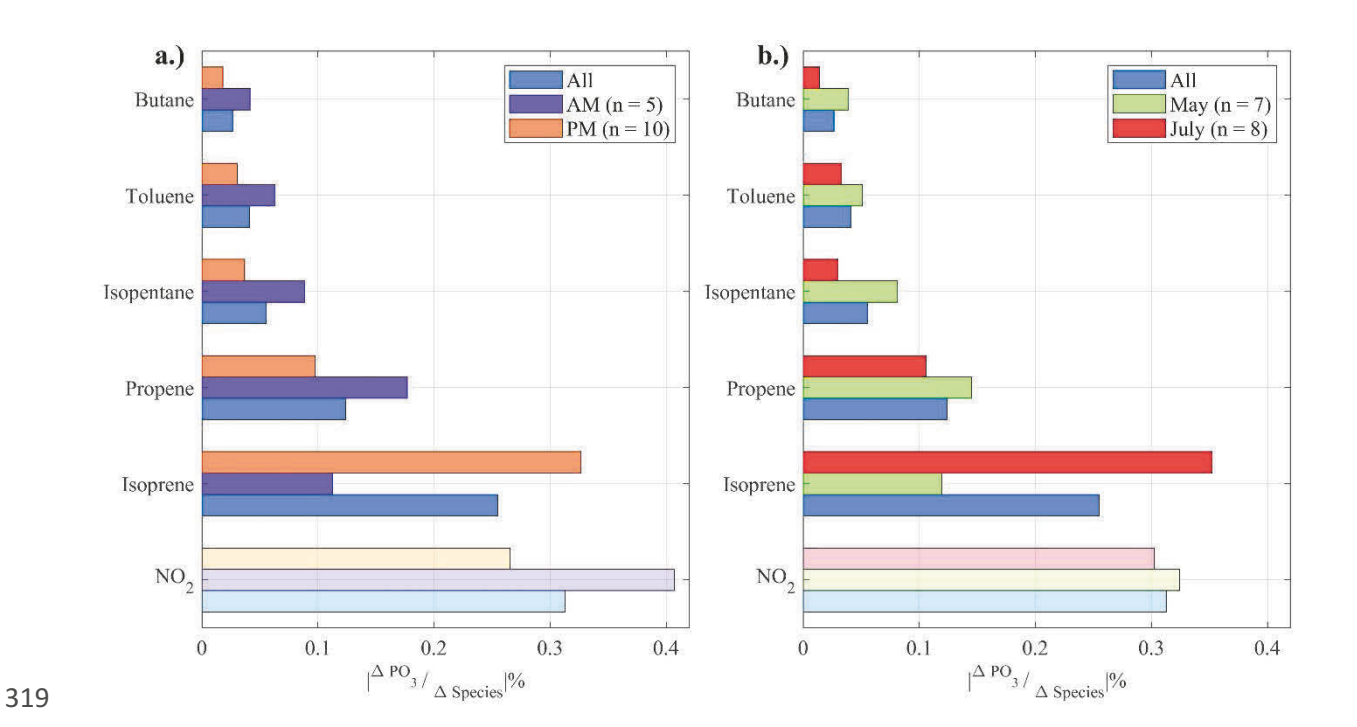


**Figure 5:** Median modeled percent PO<sub>3</sub> change per percent species change for samples with VOC-limited PO<sub>3</sub> (based on Fig. 2). Top 5 species are ranked by overall sensitivity and includes (a) AM (purple), PM (orange), and all (blue) median sensitivity and (b) May (green), July (red), and all (blue) median sensitivity. NO<sub>2</sub> sensitivity is included for comparison (Based on Fig. 2) with a transparent color to indicate the inverse relationship with PO<sub>3</sub>.

The chemical composition of the atmosphere varies diurnally and seasonally. The only VOC that exhibits greater PO<sub>3</sub> sensitivity in the afternoon than the morning is isoprene. As the day progresses, warmer afternoon temperatures contribute to greater BVOC emissions (Coates et al., 2016). A 1% change in the isoprene concentration will have a bigger impact on PO<sub>3</sub> in the afternoon (0.33%) than in the morning (0.20%). Because isoprene is highly reactive, a small increase in isoprene at greater initial concentrations will have a compounding effect on ozone production through multi-generational chemistry. Every other VOC included in Fig. 5a has a greater impact in the morning than afternoon. Of these, the ones with the biggest diurnal variations, relative to their percent change in PO<sub>3</sub> are isopentane, toluene, and butane. There is a possible nighttime buildup of these anthropogenic VOCs, due to persistent emissions as well as a lower planetary boundary layer depth which contributes to greater morning VOC concentrations

 (Ring et al., 2023). In the morning, when PO<sub>3</sub> is greatest, PO<sub>3</sub> is most sensitive to anthropogenic VOCs.

The comparison between May and July demonstrates a similar pattern. Isoprene is the only VOC in this list to have a greater impact on PO<sub>3</sub> in July than May. The difference is a factor of three; a 1% change in isoprene causes a 0.12% change in PO<sub>3</sub> in May and a 0.37% change in July. The later summer is more sensitive to BVOC while May is more sensitive to anthropogenic VOC. Supplemental Text S2 explores the sensitivity of PO<sub>3</sub> to HCHO, which is mainly a secondary product of VOC oxidation in the spring and summer and an important contributor to total OH reactivity and HO<sub>2</sub> production.

# 3.3 Chemical Mechanism Comparison

It is too computationally expensive to use explicit chemical mechanisms such as MCM in regulatory air quality models, instead condensed mechanisms such as CB6r2 are used. We repeat the previous model calculations using CB6r2 to highlight differences in model results owing to the use of this condensed chemical mechanism.

Calculated PO<sub>3</sub> is sensitive to the choice of chemical mechanism. When using MCM, PO<sub>3</sub> is 20% higher on average compared to CB6r2 (Fig. 6a). This result is consistent across all simulations ( $R^2 = 0.91$ ) and is invariant between spring and summer. Fig. 6b compares the two production terms of PO<sub>3</sub> (first two terms of Equation 5) for CB6r2 versus MCM. Ozone production from CB6r2 is 14% slower than MCM for the reaction of HO<sub>2</sub> with NO and 28% slower for RO<sub>2</sub> + NO reactions, with both channels contributing roughly equally to total PO<sub>3</sub>.

 Predicted NO is the same for both mechanisms (Fig. S8), thus differences are most likely related to radical concentrations and/or rate coefficients. Radical concentrations are 31% higher on

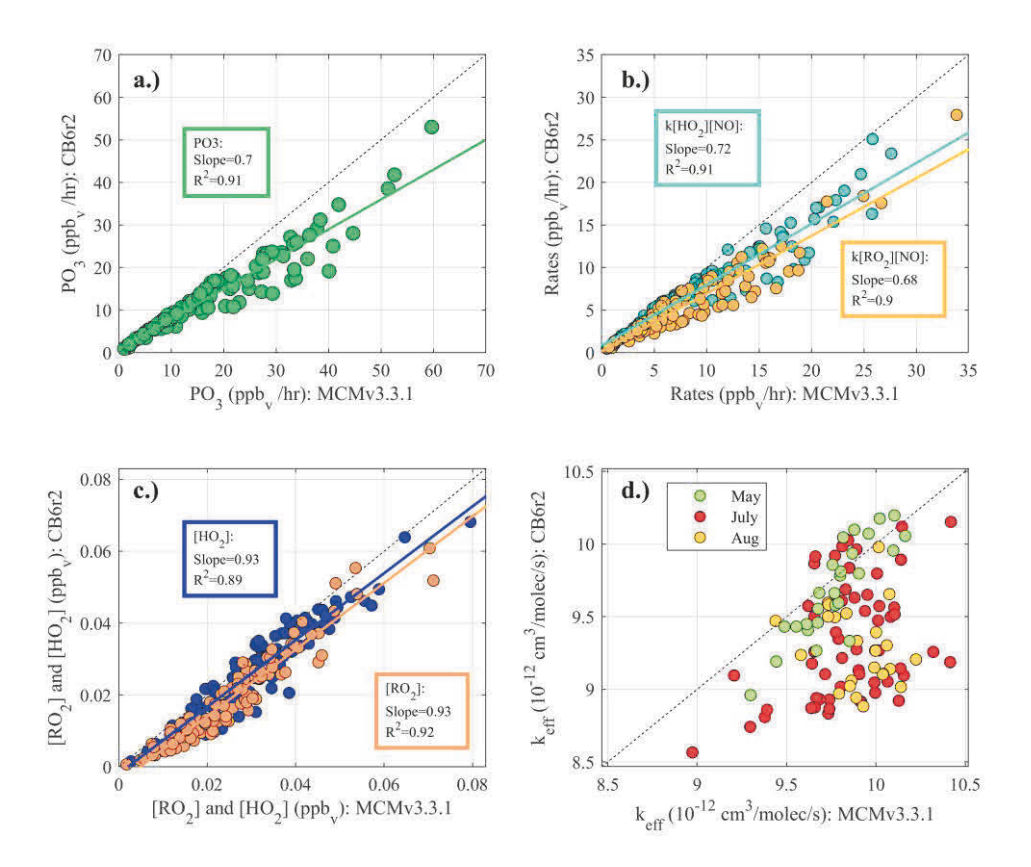


**Figure 6:** A comparison of MCMv3.3.1 to CB6r2 output: (a) instantaneous netPO<sub>3</sub> (Equation 5), (b) ozone production terms from HO<sub>2</sub> (blue) and RO<sub>2</sub> (yellow), (c) final mixing ratios of HO<sub>2</sub> (blue) and total RO<sub>2</sub> (yellow), (d) k- effective RO<sub>2</sub> + NO rate coefficient (Equation 7) colored by the month of the observation. Lines of best fit are included in panels a-c. Dashed black lines are 1:1 reference lines. average in MCM (Fig. 6c). Though the comparisons of HO<sub>2</sub> and RO<sub>2</sub> have slopes of 0.93 (Fig. 6c), there are consistent offsets between the two mechanisms as shown by a negative y-intercept (y<sub>int</sub> = -1 ppt for HO<sub>2</sub> and y<sub>int</sub> = -4 ppt for RO<sub>2</sub>).

Differences in reaction rate coefficients may also contribute to differences in PO<sub>3</sub>. The rate constant for HO<sub>2</sub> + NO is identical in both mechanisms  $(3.45 \times 10^{-12} \times e^{(270/T)})$ ; Sander et al., 2011), therefore any differences in the rate of ozone production related to HO<sub>2</sub> and NO is strictly

 due to their concentrations. To compare the rate coefficients for  $RO_2 + NO$  between mechanisms, we calculate an effective rate constant that is weighted by all individual  $RO_2$  reactions.

$$k_{eff} = \frac{\sum (k_i[NO][RO2]_i)}{[NO]\sum [RO2]_i}$$
 (7)

 $k_{eff}$  from CB6r2 is on average 96% of  $k_{eff}$  from MCM (Fig. 6d). This, along with greater total RO<sub>2</sub> concentrations, drives faster PO<sub>3</sub> in MCM. Variability of  $k_{eff}$  is slightly larger in CB6r2 than MCM (standard deviations are  $0.39\times10^{-12}$  and  $0.24\times10^{-12}$  cm<sup>3</sup>/molecules/s, respectively) suggesting the weighted rate coefficients in the lumped mechanism are more sensitive to changes in VOC distributions than in the explicit MCM.

The samples with the biggest discrepancies in  $k_{eff}$  occur in the summer ( $k_{eff,CB6r2}/k_{eff,MCM}$  = 94%), while the samples taken in May have better agreement ( $k_{eff,CB6r2}/k_{eff,MCM}$  = 99%). One possible explanation for the seasonal difference in  $k_{eff}$  between the two mechanisms is the changing distribution of  $RO_2$ . In summer, a greater portion of  $RO_2$  is BVOCs whereas in spring anthropogenic alkenes make up more of total  $RO_2$ . The effect of combining all isoprene products into a single species in CB6r2 will impact later-generation chemistry. This suggests that changing VOC distributions in urban areas may create spatial and/or seasonal bias in regional and global chemical transport models that use lumped schemes such as CB6r2. Higher  $k_{eff}$  in May is accompanied by lower total  $RO_2$  concentrations, resulting in little seasonal difference in the agreement of  $PO_3$  between MCM and CB6r2.

Fig. 7 shows median PO<sub>3</sub> curves generated using MCM (blue) and CB6r2 (green). As discussed previously, control PO<sub>3</sub> is on average 20% lower when using CB6r2 (black circles). However, the peak PO<sub>3</sub> when using CB6r2 is 41% lower than the median peak using MCM. Due to the condensed groups of peroxy radicals in CB6r2, there is less calculated OH reactivity and

 hence PO<sub>3</sub>. The median value of LRO<sub>x</sub>/LNO<sub>x</sub> at the peak of the curves is consistent with the value using MCM (0.29 and 0.30 for CB6r2 and MCM, respectively). While the total concentrations of RO<sub>2</sub> vary between the mechanisms, the ratio of radical destruction from NO<sub>x</sub> reactions to RO<sub>2</sub> self-reactions is the same. In Fig. 7 we use the value of 0.30 for the LRO<sub>x</sub>/LNO<sub>x</sub> threshold for both mechanisms (pink triangle).

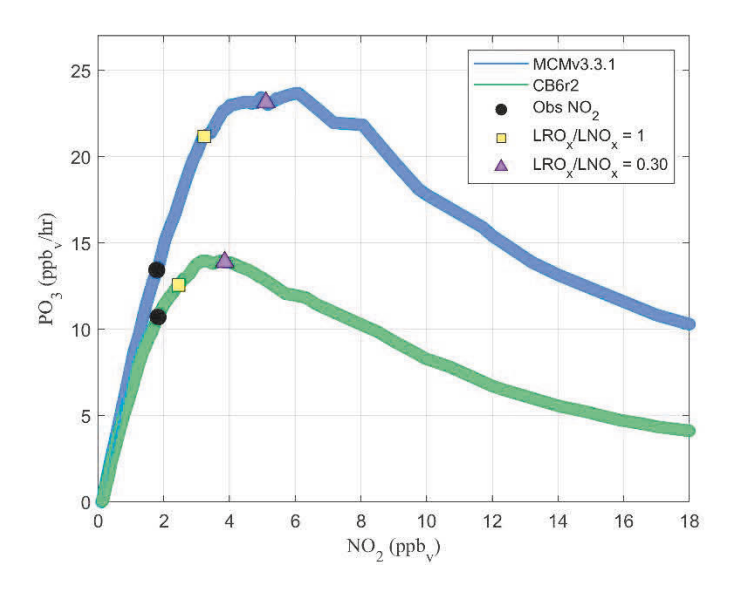
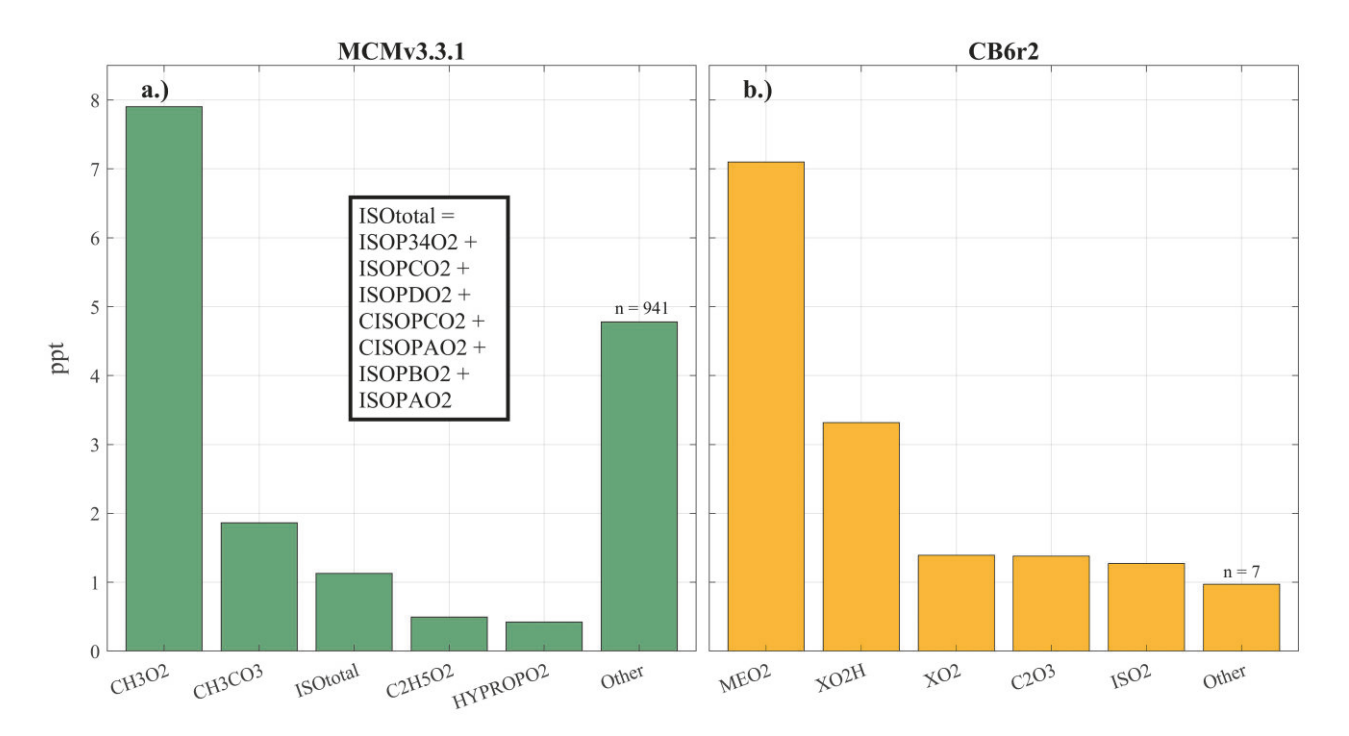


Figure 7: Median PO<sub>3</sub> (ppb/hr) as a function of initial NO<sub>2</sub> concentration using MCMv3.3.1 (blue) and CB6r2 (green). Each line includes the observed NO<sub>2</sub> (black circle), LRO<sub>x</sub>/LNO<sub>x</sub> = 1 (yellow square), and  $LRO_x/LNO_x = 0.30$  (pink triangle).

Using the same transition thresholds ( $0.3 \le LRO_x/LNO_x \le 1$ ), a greater portion of samples are in a VOC-limited regime (23%) or in transition (16%) using CB6r2. The peak of the CB6r2 ozone production curve occurs at lower NO<sub>2</sub> values, placing more samples at or beyond the peak of the curve and in the VOC-limited regime.

Fig. 8 compares the concentrations of specific RO<sub>2</sub> species between mechanisms. There are 13 subset groups in CB6r2 that react with NO (Hildebrandt Ruiz and Yarwood, 2013). The most abundant peroxy radical for both mechanisms is the methyl peroxy radical (CH<sub>3</sub>O<sub>2</sub>), which is represented explicitly as CH3O2 and MEO2 in MCM and CB6r2, respectively. On average,

 the calculated CH<sub>3</sub>O<sub>2</sub> mixing ratio is slightly greater in MCM (7.9 ppt) compared to CB6r2 (7.1 ppt). In contrast, the mixing ratio of isoprene-derived RO<sub>2</sub> is slightly greater in CB6r2 (ISO2, 1.3 ppt) than the sum of seven isomers in MCM (ISOtotal, 1.1 ppt). The sum of the top five RO<sub>2</sub> in CB6r2 (14.5 ppt) is 23% greater than in MCM (11.8 ppt). However, the sum of the remaining RO<sub>2</sub>, included as 'other' in Fig. 8, is 3.8 ppt (80%) greater in MCM. The greater total average RO<sub>2</sub> concentration using MCM shown in Fig. 8 is due to the accumulation of many minor RO<sub>2</sub> that are not explicitly represented in CB6r2.



**Figure 8:** The median concentrations of the 5 most abundant RO<sub>2</sub> and the summation of all other RO<sub>2</sub> species in **(a)** MCMv3.3.1 and **(b)** CB6r2. The seven isoprene products from OH addition given in Jenkin et al. 2015 are lumped together in MCM labeled as 'ISOtotal' for comparison with ISO2 in CB6r2.

Because OH reaction with VOC is the rate-liming step for RO<sub>2</sub> formation, OH reactivity (Equation 6) is a useful metric for VOC contributions to RO<sub>2</sub> production. Fig. 9 shows speciated OHr from MCM and CB6r2 split into three groups: measured inorganics (green), measured organics (blue) and model-generated species (red) where each bar is an individual compound (or lumped group in the case of CB6r2). Modeled total OHr is 20% greater in MCM than CB6r2 (6.0

 vs 5.0 s<sup>-1</sup>). The contribution of measured inorganics is 6% lower in CB6r2 (MCM: 1.8 s<sup>-1</sup>; CB6r2 1.7 s<sup>-1</sup>), likely due to slight differences in rate coefficients. The contribution of measured organics is 13% lower in CB6r2 (MCM: 1.5 s<sup>-1</sup>; CB6r2: 1.3 s<sup>-1</sup>) due to species grouping in the latter. Model-generated secondary VOC explains most of the difference in total OHr. The model-generated group accounts for 45% and 40% of total OHr for MCM and CB6r2, respectively. We calculate 2.7 s<sup>-1</sup> from 2215 species in MCM and 2.0 s<sup>-1</sup> from 32 lumped or explicit species in CB6r2, a difference of 26%. Results using both mechanisms exhibit similar rankings of the most reactive species in the model-generated species category. The largest model-generated contributors to OH reactivity include HCHO, acetaldehyde, first-generation isoprene oxidation products (methyl vinyl ketone and methacrolein), and glyoxal.

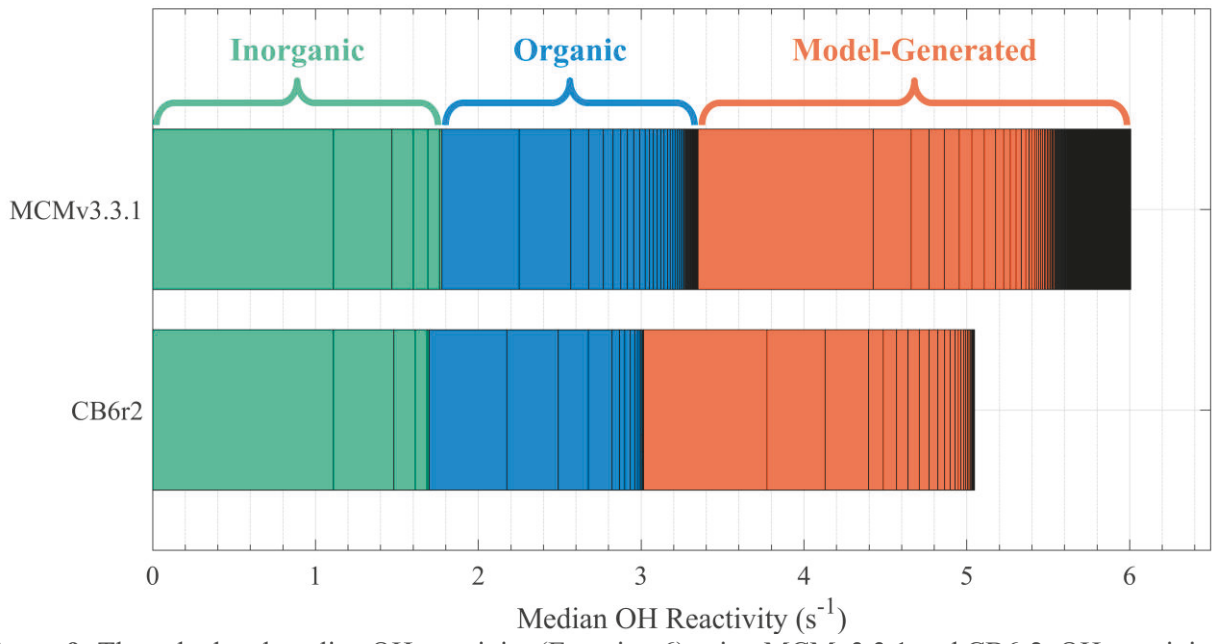


**Figure 9:** The calculated median OH reactivity (Equation 6) using MCMv3.3.1 and CB6r2. OH reactivity is separated by individual species and grouped by inorganic measured species (CO, NO<sub>2</sub>, NO, SO<sub>2</sub>, and O<sub>3</sub> in green), organic measured VOC (blue), and model-generated species (orange). MCMv3.3.1 has a total of 66 measured species and 2215 modeled species. CB6r2 includes 19 measured species and 32 modeled species.

Of the MCM model-generated species, 99% have an OHr less than 0.01 s<sup>-1</sup>, but together those species make up 20% of the overall model-generated OHr. Thus, secondary reaction products have a cumulatively significant impact on the total calculated ozone production. Measurements of speciated oxygenated VOC (oVOC), total OH reactivity and total RO<sub>2</sub>/HO<sub>2</sub> concentrations would be valuable to validate these results in future studies.

# 4. Conclusions

We use aircraft observations from the LISTOS campaign to estimate PO<sub>3</sub> in the New York City area in the spring and summers of 2017-2019. We first classify the PO<sub>3</sub> regime by the response of PO<sub>3</sub> to initial NO<sub>2</sub> concentrations and find that 14% of air samples are in a VOClimited regime. A transition between PO<sub>3</sub> regimes, defined as  $0.3 \le LRO_x/LNO_x \le 1$ , encompasses 16% of the data. In this range, PO<sub>3</sub> increases with increasing NO<sub>x</sub> but is more sensitive (per molecule) to VOCs. Samples in a transition or in a VOC-limited regime are primarily located along the coast of Connecticut and in New York City. Using the LRO<sub>x</sub>/LNO<sub>x</sub> ratio to determine PO<sub>3</sub> regime indicates a higher portion of samples are VOC-limited as compared to only using the slope of the PO<sub>3</sub> isopleths to make this determination.

PO<sub>3</sub> exhibits diurnal and seasonal variations with maximum potential PO<sub>3</sub> being greater in the morning than the afternoon due to higher VOC concentrations in a shallower boundary layer. May is more likely to be VOC-limited (27% of samples) than July (14% of samples) or August (no samples), which is likely due to changes in total VOC availability rather than changing NO<sub>x</sub> concentrations.

For samples within a VOC-limited regime, sensitivity tests reveal that isoprene concentrations have the greatest impact on PO<sub>3</sub>, with a strong diurnal and seasonal variation. In the afternoon, PO<sub>3</sub> is most sensitive to isoprene, while in the morning, anthropogenic alkenes have a bigger effect on PO<sub>3</sub>.

In the spring, focusing regulatory efforts on VOC reductions accompanied by NO<sub>x</sub> reductions would most efficiently reduce PO<sub>3</sub> in this region. As temperatures warm, the ozone season is extending earlier into the spring (Ring et al., 2023). Therefore, ozone reduction strategies should be designed based on seasonal and diurnal differences in VOC concentrations and distributions.

We calculate PO<sub>3</sub> using CB6r2 for a more direct comparison to regulatory air quality models that use lumped schemes. We find that using CB6r2 reduces PO<sub>3</sub> and OH reactivity by 20% compared to results using MCMv3.3.1. These differences stem from assumptions regarding the photochemical kinetic parameters for the lumped RO<sub>2</sub> families. The value of LRO<sub>x</sub>/LNO<sub>x</sub> at the peak of these curves remains the same indicating the relative rates of radical destruction due to NO<sub>x</sub> reactions and radical-self reactions are consistent between mechanisms. Using CB6r2, more samples are in a VOC-limited regime due to peak PO<sub>3</sub> occurring at lower values of NO<sub>2</sub>.

The largest discrepancy in the OH reactivity comes from model-generated species, the most abundant of which include formaldehyde, acetaldehyde, first-generation isoprene oxidation products (methyl vinyl ketone and methacrolein), and glyoxal. Future observations of such oxidation products would provide important constraints in the calculation of PO<sub>3</sub> and improve confidence in our understanding of ozone production regimes. Volatile chemical products, which were not measured during LISTOS, are an increasingly important class of VOC and have been shown to increase modeled PO<sub>3</sub> by at least 10% (Coggon et al., 2021; Gkatzelis et al., 2021).

Our analysis of the VOCs observed during LISTOS shows spatial and temporal variations in PO<sub>3</sub> chemistry in densely populated areas. We emphasize that future aircraft field campaigns should measure a wide suite of VOCs, including HCHO, to provide a more detailed understanding of PO<sub>3</sub> chemistry. Implementing a more accurate representation of atmospheric chemical processes ensures the efficacy of regulatory models used to develop air quality policy.

# 5. Competing Interests

The authors declare that they have no competing financial interests or personal relationships that could have appeared to influence the work reported in this paper.

# 6. CRediT authorship contribution statement

- Abby E Sebol: Conceptualization, Methodology, Software, Formal analysis, Investigation,
- Writing original draft, Visualization.
- **Timothy P Canty:** Conceptualization, Methodology, Resources, Writing review & editing,
- Funding acquisition.
- Glenn M. Wolfe: Software, Conceptualization, Methodology, Resources, Writing review & **500** 
  - editing, Funding acquisition.
  - **Reem Hannun:** Conceptualization, Methodology, Resources, Writing review & editing.
  - **Allison M. Ring:** Conceptualization, Methodology, Resources, Writing review & editing.
- **Xinrong Ren:** Investigation, Data curation, Writing review & editing. **504**

### 7. Acknowledgements

- We thank the National Science Foundation for support of the grant AGS-2023605, Maryland
- Department of the Environment (MDE) for support of the Regional Atmospheric Measurement
- Modeling and Prediction Program (RAMMPP; Grant # U00P3600274), the National Aeronautics
- and Space Administration (NASA) for support of the Atmospheric Composition Campaign Data
- Analysis and Modeling grant (ACCDAM; Grant # 80NSSC21K1448), and the North East States
- for Coordinated Air Use Management (NESCAUM; Grant # NESCAUMUMDTSA20190603).

- 514 (https://www-air.larc.nasa.gov/cgi-bin/ArcView/listos?UMD-AIRCRAFT=1) last accessed
- 6 January 2023. We thank Jason St. Clair for the CAFE data and Phil Stratton for assistance in data 515 7
- 8 516 collection during the research flights. Finally, we thank Ross Salawitch, Russell Dickerson, and
  - Akanksha Singh for their help in conceptualization, methodology, and visualization. 517

<sup>11</sup> 518 12

519

521

19 **522** 

20 **523** 21 **524** 

<sup>22</sup> **525** 

25 **527** 

26 **528** 27

31 **532** 32 **533** 

37 **537** <sup>38</sup> **538** 

42 **541** 43 **542** 

48 **546** <sup>49</sup> **547** 

<sup>50</sup> **548** 

53 **550** 54 **551** 

<sup>55</sup> **552** 

<sub>58</sub> **554** 59 **555** 

60 556

549

553

526

529

530

534

535

539

540

543

544

5

9

10

13 14

15 <sup>16</sup> 520

17

18

23

24

28

29 30 **531** 

33

34

35 36 **536** 

39

40

41

44

45

46 47 **545** 

51

52

56

57

61 62

63 64 65

# 8. References

- Anenberg, S. C., L. W. Horowitz, D. Q. Tong, and J. J. West, 2010: An Estimate of the Global Burden of Anthropogenic Ozone and Fine Particulate Matter on Premature Human Mortality Using Atmospheric Modeling. Environmental Health Perspectives, 118, 1189-1195.
  - Atkinson, R., D. L. Baulch, R. A. Cox, J. N. Crowley, R. F. Hampson, R. G. Hynes, M. E. Jenkin, M. J. Rossi, and J. Troe, 2004: Evaluated kinetic and photochemical data for atmospheric chemistry: Volume I - gas phase reactions of O-x, HOx, NOx and SOx species. Atmos. Chem. Phys., 4, 1461-1738.
  - Atkinson, R., D. L. Baulch, R. A. Cox, J. N. Crowley, R. F. Hampson, R. G. Hynes, M. E. Jenkin, M. J. Rossi, and J. Troe, 2006: Evaluated kinetic and photochemical data for atmospheric chemistry: Volume II - gas phase reactions of organic species. Atmos. Chem. Phys., 6, 3625-4055.
  - Baier, B. C., W. H. Brune, B. L. Lefer, D. O. Miller, and D. K. Martins, 2015: Direct ozone production rate measurements and their use in assessing ozone source and receptor regions for Houston in 2013. Atmospheric Environment, 114, 83-91.
  - Chen, S., X. Ren, J. Mao, and Coauthors, 2010: A comparison of chemical mechanisms based on TRAMP-2006 field data. Atmospheric Environment, 44, 4116-4125.
  - Chen, X., D. B. Millet, H. B. Singh, and Coauthors, 2019: On the sources and sinks of atmospheric VOCs: an integrated analysis of recent aircraft campaigns over North America. Atmos. Chem. Phys., 19, 9097-9123.
  - Coates, J., K. A. Mar, N. Ojha, and T. M. Butler, 2016: The influence of temperature on ozone production under varying NOx conditions – a modelling study. Atmos. Chem. Phys., 16, 11601-11615.
  - Coggon, M. M., G. I. Gkatzelis, B. C. McDonald, and Coauthors, 2021: Volatile chemical product emissions enhance ozone and modulate urban chemistry. Proceedings of the National Academy of Sciences of the United States of America, 118.
  - Couillard, M. H., M. J. Schwab, J. J. Schwab, and Coauthors, 2021: Vertical Profiles of Ozone Concentrations in the Lower Troposphere Downwind of New York City During LISTOS 2018–2019. Journal of Geophysical Research: Atmospheres, 126.
  - Crawford, J., D. Davis, J. Olson, and Coauthors, 1999: Assessment of upper tropospheric HOx sources over the tropical Pacific based on NASA GTE/PEM data: Net effect on HOx and other photochemical parameters. J. Geophys. Res.-Atmos., 104, 16255-16273.
  - EPA: Summary Nonattainment Area Population Exposure Report. [Available online at https://www3.epa.gov/airquality/greenbook/popexp.html.]
  - Gery, M. W., G. Z. Whitten, J. P. Killus, and M. C. Dodge, 1989: A photochemical kinetics mechanism for urban and regional scale computer modeling. Journal of Geophysical Research: Atmospheres, 94, 12925-12956.

**577** 

46 591

**596** 

**564** 

18 568

**569 570** 

<sup>21</sup> **571** 

**573** 

**574** <sup>26</sup> **575** 

**578** <sup>31</sup> **579** 

**583** 

41 587 

**592 593** 

**597** 

- Gkatzelis, G. I., M. M. Coggon, B. C. McDonald, J. Peischl, K. C. Aikin, J. B. Gilman, M. Trainer, and C. Warneke, 2021: Identifying Volatile Chemical Product Tracer Compounds in US Cities. Environmental Science & Technology, **55**, 188-199.
  - He, H., X. Z. Liang, C. Sun, Z. N. Tao, and D. Q. Tong, 2020: The long-term trend and production sensitivity change in the US ozone pollution from observations and model simulations. Atmos. Chem. Phys., 20, 3191-3208.
  - Hildebrandt Ruiz, L., and G. Yarwood, 2013: Interactions between organic aerosol and NOy: Influence on oxidant production. University of Texas at Austin and ENVIRON International Corporation, 12-012.
  - Jenkin, M. E., J. C. Young, and A. R. Rickard, 2015: The MCM v3.3.1 degradation scheme for isoprene. Atmos. Chem. Phys., 15, 11433-11459.
  - Kleinman, L. I., P. H. Daum, Y. N. Lee, L. J. Nunnermacker, S. R. Springston, J. Weinstein-Lloyd, and J. Rudolph, 2001: Sensitivity of ozone production rate to ozone precursors. Geophys. Res. Lett., 28, 2903-2906.
  - Lindsay, A. J., D. C. Anderson, R. A. Wernis, and Coauthors, 2022: Ground-based investigation of HOx and ozone chemistry in biomass burning plumes in rural Idaho. *Atmos. Chem.* Phys., 22, 4909-4928.
  - Loughner, C. P., M. Tzortziou, M. Follette-Cook, and Coauthors, 2014: Impact of Bay-Breeze Circulations on Surface Air Quality and Boundary Layer Export. Journal of Applied *Meteorology and Climatology*, **53**, 1697-1713.
  - Malley, C. S., D. K. Henze, J. C. I. Kuylenstierna, H. W. Vallack, Y. Davila, S. C. Anenberg, M. C. Turner, and M. R. Ashmore, 2017: Updated Global Estimates of Respiratory Mortality in Adults >= 30 Years of Age Attributable to Long-Term Ozone Exposure. *Environmental* Health Perspectives, 125.
  - Mao, J., X. Ren, S. Chen, and Coauthors, 2010: Atmospheric oxidation capacity in the summer of Houston 2006: Comparison with summer measurements in other metropolitan studies. Atmospheric Environment, 44, 4107-4115.
  - Marvin, M. R., G. M. Wolfe, R. J. Salawitch, and Coauthors, 2017: Impact of evolving isoprene mechanisms on simulated formaldehyde: An inter-comparison supported by in situ observations from SENEX. Atmospheric Environment, 164, 325-336.
  - Mazzuca, G. M., K. E. Pickering, D. A. New, J. Dreessen, and R. R. Dickerson, 2019: Impact of bay breeze and thunderstorm circulations on surface ozone at a site along the Chesapeake Bay 2011–2016. Atmospheric Environment, 198, 351-365.
  - Mazzuca, G. M., X. Ren, C. P. Loughner, M. Estes, J. H. Crawford, K. E. Pickering, A. J. Weinheimer, and R. R. Dickerson, 2016: Ozone production and its sensitivity to NOx and VOCs: results from the DISCOVER-AO field experiment, Houston 2013. Atmos. Chem. Phys., 16, 14463-14474.
  - Mazzuca, G. M., K. E. Pickering, R. D. Clark, C. P. Loughner, A. Fried, D. C. Stein Zweers, A. J. Weinheimer, and R. R. Dickerson, 2017: Use of tethersonde and aircraft profiles to study the impact of mesoscale and microscale meteorology on air quality. Atmospheric Environment, 149, 55-69.
  - McDonald, B. C., J. A. de Gouw, J. B. Gilman, and Coauthors, 2018: Volatile chemical products emerging as largest petrochemical source of urban organic emissions. Science, 359, 760-764.

46 635

47 636 

**640** 

**641** 

**627** 

18 612

**613** 20 614

24 617

**618** <sup>26</sup> **619** 

**622 623** 

- Newsome, B., and M. Evans, 2017: Impact of uncertainties in inorganic chemical rate constants on tropospheric composition and ozone radiative forcing. Atmos. Chem. Phys., 17, 14333-14352.
  - Oliveira, K., M. Guevara, O. Jorba, X. Querol, and C. P. Garcia-Pando, 2023: A new NMVOC speciated inventory for a reactivity-based approach to support ozone control strategies in Spain. Science of the Total Environment, 867.
  - Olson, J. R., J. H. Crawford, D. D. Davis, and Coauthors, 2001: Seasonal differences in the photochemistry of the South Pacific: A comparison of observations and model results from PEM-Tropics A and B. J. Geophys. Res.-Atmos., 106, 32749-32766.
  - Olson, J. R., J. H. Crawford, G. Chen, and Coauthors, 2004: Testing fast photochemical theory during TRACE-P based on measurements of OH, HO2, and CH2O. J. Geophys. Res.-Atmos., 109.
  - Ren, X. R., O. E. Salmon, J. R. Hansford, and Coauthors, 2018: Methane Emissions From the Baltimore-Washington Area Based on Airborne Observation: Comparison to Emissions Inventories. J. Geophys. Res.-Atmos., 123, 8869-8882.
  - Ring, A. M., R. R. Dickerson, A. E. Sebol, X. Ren, S. E. Benish, R. J. Salawitch, A. Galasyn, and P. J. Miller, 2023: Anthropogenic VOCs in the Long Island Sound, NY Airshed and their role in ozone production. Atmospheric Environment, 296, 119583.
  - Roberts, S. J., R. J. Salawitch, G. M. Wolfe, M. R. Marvin, T. P. Canty, D. J. Allen, D. L. Hall-Quinlan, D. J. Krask, and R. R. Dickerson, 2022: Multidecadal trends in ozone chemistry in the Baltimore-Washington Region. Atmospheric Environment, 285.
  - Sander, R., A. Baumgaertner, S. Gromov, and Coauthors, 2011: The atmospheric chemistry box model CAABA/MECCA-3.0. Geoscientific Model Development, 4, 373-380.
  - Schroeder, J. R., J. H. Crawford, A. Fried, and Coauthors, 2017: New insights into the column CH2O/NO2 ratio as an indicator of near-surface ozone sensitivity. J. Geophys. Res.-Atmos., 122, 8885-8907.
  - Schroeder, J. R., J. H. Crawford, A. Fried, and Coauthors, 2016: Formaldehyde column density measurements as a suitable pathway to estimate near-surface ozone tendencies from space. J. Geophys. Res.-Atmos., 121, 13088-13112.
  - Souri, A. H., C. R. Nowlan, G. M. Wolfe, and Coauthors, 2020: Revisiting the effectiveness of HCHO/NO2 ratios for inferring ozone sensitivity to its precursors using high resolution airborne remote sensing observations in a high ozone episode during the KORUS-AQ campaign. Atmospheric Environment, 224.
  - St Clair, J. M., A. K. Swanson, S. A. Bailey, and T. F. Hanisco, 2019: CAFE: a new, improved nonresonant laser-induced fluorescence instrument for airborne in situ measurement of formaldehyde. Atmospheric Measurement Techniques, 12, 4581-4590.
  - Strode, S. A., J. R. Ziemke, L. D. Oman, L. N. Lamsal, M. A. Olsen, and J. Liu, 2019: Global changes in the diurnal cycle of surface ozone. Atmospheric Environment, 199, 323-333.
  - Wolfe, G. M., M. R. Marvin, S. J. Roberts, K. R. Travis, and J. Liao, 2016: The Framework for 0-D Atmospheric Modeling (F0AM) v3.1. Geoscientific Model Development, 9, 3309-3319.
  - Yang, X. Y., B. Yuan, Z. Peng, Y. W. Peng, C. H. Wu, S. X. Yang, J. Li, and M. Shao, 2022: Intercomparisons of VOC oxidation mechanisms based on box model: A focus on OH reactivity. Journal of Environmental Sciences, 114, 286-296.